Histogram analysis as a method for determining the line tension by Monte-Carlo simulations

Y.S.Djikaev*
Department of Chemistry, Baker Laboratory, Cornell University
Ithaca, New York 14853-1301

Abstract

A method is proposed for determining the line tension, which is the main physical characteristic of a three-phase contact region, by Monte-Carlo (MC) simulations. The key idea of the proposed method is that if a three-phase equilibrium involves a three-phase contact region, the probability distribution of states of a system as a function of two order parameters depends not only on the surface tension, but also on the line tension. This probability distribution can be obtained as a normalized histogram by appropriate MC simulations, so one can use the combination of histogram analysis and finite-size scaling to study the properties of a three phase contact region. Every histogram and results extracted therefrom will depend on the size of the simulated system. Carrying out MC simulations for a series of system sizes and extrapolating the results, obtained from the corresponding series of histograms, to infinite size, one can determine the line tension of the three phase contact region and the interfacial tensions of all three interfaces (and hence the contact angles) in an infinite system. To illustrate the proposed method, it is applied to the three-dimensional ternary fluid mixture, in which molecular pairs of like species do not interact whereas those of unlike species interact as hard spheres. The simulated results are in agreement with expectations.

*E-mail:id45@cornell.edu

1 Introduction

If two bulk phases are in equilibrium, the profiles of the order parameter (distinguishing between the phases) in the planar interface between them are non-uniform. Due to this non-uniformity, excess contributions to the extensive thermodynamic parameters of the system arise. These are usually referred to the dividing surface chosen within the interfacial region. An excess quantity per unit area of the dividing surface is called a surface adsorption. All surface adsorptions but one depend on the choice of the dividing surface. The special surface adsorption is that of the grand canonical potential, and is called the surface (or interfacial) tension; it does not depend on the choice of the dividing surface (in the case of a planar interface).

The interfacial tension between coexisting phases plays a fundamental role in a theory of wetting phenomena and phase transitions. Various theoretical, numerical, and computational techniques exist for its calculation. Besides the mechanical definition of the surface tension, there are two statistical-mechanical recipes usually referred to as the virial route[1] and direct correlation function route (see, e.g., chapter 4 of ref.2). The latter is the more rigorous because it has no restrictions while the former is restricted to fluids with pair-wise additive intermolecular potentials. Although not easy in a general case, the equivalence of both methods can be proven (see, e.g., chapter 4 in ref.2 and references therein). These methods require the knowledge of the pair (and higher order) intermolecular potentials and the corresponding distribution functions in the interfacial region, which are not easy to obtain without drastic approximations.[2]

A more successful and traditional (although semi-numerical) way of calculating the surface tension is offered by density functional theory[2−4] which allows one to find the excess grand canonical potential associated with the interface between coexisting phases. This method has its own conceptual difficulties (see, e.g.,refs.3-5) related to (a) the choice of free-energy density for intermediate (between two bulk) values of the order parameter, particularly in the critical region where fluctuations are important, and (b) the long-

wavelength interface instability due to capillary waves.[6]

Finally, there is a variety of computer simulation techniques for calculating the surface tension. In the case of a system of continuous potentials the majority of simulations have used the mechanical definition[1] of the surface tension and the virial expressions for the normal and tangential components of the pressure tensor.[7−9] The results obtained via these simulations show a large scatter.[10] Another simulation method involves the direct calculation of the free energy change in forming an interface.[11,12] In simulation of lattice models a wider variety of methods has been used including thermodynamic integration using a biasing field to force the formation of the interface[13−15] and calculating the free energy differences for systems with periodic and anti-periodic boundary conditions.[16,17]

All these methods implicitly or explicitly include conditions restricting the interfacial configuration space that can be sampled in simulations. Many of the methods also require establishing a well-defined interfacial region which can be quite difficult, particularly under conditions close to a critical point where the interface becomes very diffuse. An alternative approach to calculating the surface tension was proposed by Binder,[18] whose method is based on the analysis of the probability distribution of states of a system as a function of the order parameter obtained from Monte-Carlo simulations as a normalized histogram. Under conditions where two phases can coexist in equilibrium, the histogram has two peaks each of which corresponds to a homophase state, i.e., to the whole system being in one of the two phases (Figure 1). Intermediate values of the order parameter correspond to heterophase states such that one part of the system is in one phase while the rest is in the other phase. The key idea of Binder's method consists of establishing a relation between the minimum of the histogram and the interfacial tension between two coexisting phases. A simulated histogram gives the interfacial tension of the finite-size (simulated) system, and the interfacial tension of the infinite system is obtained by extrapolating a series of results for systems of different sizes (but otherwise for the same thermodynamic conditions) to infinite size. Binder's method has been successfully applied to a wide

variety of models.[18−31]

If three phases are in equilibrium, there may exist a three-phase contact region in addition to three two-phase interfaces. The distortion of the order parameter(s) profile(s) in the three-phase contact region gives rise to excess contributions to the extensive thermodynamic characteristics of the system. These are usually referred to the three-phase contact line". Excess quantities per unit length of the contact line are called linear adsorptions. For three bulk phases in equilibrium, the interfaces between them can be treated as planar and the line of their intersection, that is, the contact line, as a straight line, so that its spatial location is determined by two coordinates in the plane perpendicular to it. The location of the contact line is arbitrary and among all linear adsorptions only one does not depend on its choice. This is the linear adsorption of the grand canonical potential also called the line tension.[2] All other adsorptions depend on the location of the contact line and hence are functions of its two coordinates. It should be noted that line tension may be positive or negative,[2] unlike surface tension that is always positive.

The line tension has been studied to a much lesser extent than the surface tension both experimentally and theoretically.[32−34,2,35−40] There are no general statistical mechanical expressions for calculating the line tension that would be equivalent to the virial and direct correlation function routes in a theory of surface tension. For the case of two fluid phases in contact with a solid surface, a statistical mechanical theory for the line tension was proposed by Tarazona and Navascués;[41] using several assumptions about molecular interactions, they derived an expression for the line tension involving the one- and two-molecule distribution functions. All other microscopic models for the line tension were based on the local density approximation of density functional theory[2,36−40] and are hence subject to conceptual problems similar to those for the surface tension.[3−5] As for computer simulation methods, they have often been applied to three-phase equilibria and wetting phenomena,[42−46] but we are not aware of direct molecular simulations of the line tension, which is probably partly due to the lack of a general statistical-mechanical theory thereof. It should be noted, however,

that studying a solid spherical particle at a liquid-vapor interface by molecular dynamics (MD) simulations and thus finding the contact angle and all interfacial tensions involved, Bresme and Quirke[43] evaluated the (particle-liquid-vapor) line tension with the help of a phenomenological expression for the particle free energy (found also by MD simulations) and modified Young's equation.

In the present paper a method is proposed for calculating the line tension by MC simulations. The method is based on the statistical-mechanical analysis of the histogram of a system under conditions of three phase equilibrium involving a three-phase contact region. The paper is structured as follows. Section 2 outlines the original histogram analysis method for determining the interfacial tension of a two-phase interface pioneered by Binder.[18] Section 3 presents a general idea of how that method can be extended to three-phase equilibria in order to determine the line tension. Section 4 discusses a general set-up of MC simulation cell and boundary conditions and there is also developed a theoretical basis for the concrete realization of the key idea in a three-dimensional ternary fluid mixture, in which molecular pairs of like species do not interact while those of unlike species interact as hard spheres;[47−49] in this model a three-phase contact region may exist at densities above the "quadruple point" density.[47−49] The details of MC simulations and results for the surface and line tensions associated with the three-phase contact region are also presented in section 4. The results are discussed and conclusions are summarized in section 5.

2 Binder's approach to determining the surface tension by Monte-Carlo simulations

Binder's method[18] for determining the interfacial tension of two coexisting phases is based on the order-parameter distribution formalism. Rather than set up an explicit interface in the MC-simulated system, this approach relies on spontaneous fluctuations that give rise to density inhomogeneities, which provide infor-

mation about the interfacial properties. The method has its own implementation difficulties,[29,31] especially far away from the critical point, but they can all be alleviated by using special sampling techniques.[23,31,50]

Consider a finite "cube-shaped" system (to be simulated) of volume L^d (d is the dimensionality) with periodic boundary conditions (PBC), which are necessary in order to avoid additional surface effects that can arise from the system boundaries. Under appropriate thermodynamic conditions (e.g., below the critical temperature if the temperature is a relevant thermodynamic parameter) the system will phase separate into phases α and β with the values m_α and m_β of the order parameter m. In a liquid-gas system the order parameter is the density; in a binary mixture of species A and B with a miscibility gap the order parameter is the mole fraction of one of the components in the coexisting A-rich and B-rich phases; in an Ising model, the order parameter is the spontaneous magnetization (two orientations thereof corresponding to the two phases). In all cases some conjugate field variable (the chemical potential, or the difference in chemical potentials of two components, or the magnetic field, respectively) has to be fixed at such a value that would correspond to coexisting phases in the thermodynamic limit.

According to the theory of equilibrium fluctuations,[51] if the system is in a pure phase with the average order parameter $\bar{m}$, the probability $p(m)$ to find the system (with $L \to \infty$) in a state with the order parameter m is given by the Gaussian distribution,

$$p(m) = L^{d/2}(2\pi kT\chi)^{-1/2} \exp[-(m-\bar{m})^2 L^d/(2kT\chi)], \tag{1}$$

where k is the Boltzmann constant, T is the temperature, and χ is the partial derivative of the order parameter with respect to its conjugate field variable, with all other variables of state of the system being fixed. For the system at coexistence where both pure phases are equally likely to occur, the probability distribution of the order parameter can be represented as the sum of two displaced Gaussians,

$$p(m) \;=\; \frac{1}{2} L^{d/2}(2\pi kT\chi_\alpha)^{-1/2} \exp[-(m-m_\alpha)^2 L^d/(2kT\chi_\alpha)]$$

$$+ \quad \frac{1}{2}L^{d/2}(2\pi kT\chi_\beta)^{-1/2}\exp[-(m-m_\beta)^2L^d/(2kT\chi_\beta)], \tag{2}$$

where χ_α and χ_β are the susceptibilities in the pure phases α and β. It is clear from eq.(2) that the probability of a *homogeneous* state with the order parameter $m_{\text{min}} = (m_\alpha + m_\beta)/2$ decreases exponentially with the volume of L^d of the system. On the other hand, the probability of *heterogeneous* fluctuations, such that two phases coexist in the system, decreases exponentially[18,56] with the interface area $2L^{d-1}$,

$$p(m_{\text{min}}^{\text{ht}}) \propto p(m_o)\exp[-2\sigma L^{d-1}/kT], \tag{3}$$

where the superscript "ht" stands for "heterogeneous", the subscript "*o*" indicates either of the pure phases α or β, and σ is the interfacial tension in an infinite system. The size dependence of the pre-exponential factor $p(m_o) \simeq \frac{1}{2}L^{d/2}(2\pi kT\chi_o)^{-1/2}$ is much weaker than the exponential one. Thus, for large enough L, the probability of "homophase" fluctuations with intermediate values m_{min} of the order parameter is negligible in comparison with the probability of "heterophase" fluctuations.

As pointed out by Binder,[18] the size dependence of the pre-exponential factor in eq.(3) can be more complicated than that contained in $p(m_o)$, due to finite-size contributions to the interfacial free energy arising, e.g., from the "Goldstone modes" and capillary waves. As a result, one can expect that for large L the probability distribution $p(m_{\text{min}})$ (the superscript "ht" is omitted henceforth) has the general form

$$p(m_{\text{min}}) = aL^x p(m_o)\exp[-2\sigma L^{d-1}/kT] \tag{4}$$

with unknown a and x, whence it follows that

$$\frac{1}{2L^{d-1}}\ln\frac{p(m_o)}{p(m_{\text{min}})} = \frac{\sigma}{kT} + b\frac{\ln L}{L^{d-1}} + c\frac{1}{L^{d-1}}, \tag{5}$$

(with unknown b and c) and

$$\frac{\sigma}{kT} = \lim_{L\to\infty}\frac{1}{2L^{d-1}}\ln\frac{p(m_o)}{p(m_{\text{min}})}. \tag{6}$$

This limit cannot be found analytically, but the probability distribution as a function of the order parameter, $p(m_o)$, can be obtained for a series of L's via appropriate MC simulations. Then, one can plot the LHS of eq.(5) vs $\ln L/L^{d-1}$ and the intercept of this plot with the ordinate axis will provide the ratio σ/kT for the interfacial tension in the infinite system.

3 Three-phase equilibrium: determination of the surface and line tensions by the histogram analysis method

If the system is under such conditions that three phases can coexist in equilibrium, there are necessarily two order parameters such that at least one in the pair differs in different phases. For example, in a single component system at the triple point the gas, liquid, and solid phases can coexist, and a pair of order parameters can be the density and a structure parameter. In some two component systems ("solvent-solute") under appropriate conditions one can observe the coexistence of three fluid phases: solvent liquid, solvent vapor, and solute liquid.[30] In such systems the densities of the components serve as a pair of order parameters. For such systems, the probability distribution of states is a function of two independent order parameters and determines a three-dimensional surface, hereafter referred to as a histogram (as in a single order parameter case). This three-dimensional surface has three peaks of equal height corresponding to three pure phases.

Consider a three component fluid system of species 1, 2, and 3. Under appropriate conditions, such a system can phase-separate (demix) into three equilibrium phases differing from each other by a pair of independent order parameters, e.g., the mole fractions of any two components, say, m_1 and m_2 (the third mole fraction is not an independent variable, $m_3 = 1 - m_1 - m_2$). Denote by $p(m_1, m_2)$ the probability distribution of states of this system with respect to the order parameters m_1 and m_2. Figure 2a presents an example of the histogram (three dimensional surface determined by the function $p(m_1, m_2)$) generated

by semigrand canonical MC simulations in a cubic box with PBC for the three-dimensional ternary fluid mixture, in which molecular pairs of like species do not interact and those of unlike species interact as hard spheres (for details see section 4). Figure 2b shows the projection of the same surface onto the mole-fraction plane. The peaks of the histogram correspond to the pure phases, say, α, β, and γ. The projections of the peaks are shown as the points o_1; $(o_1 = \alpha, \beta, \gamma)$ in Fig.2b. Their coordinates $m_i^{o_1}$ $(i = 1, 2)$ determine the composition (i.e. mole fractions) of the system in pure phases α, β, and γ. If all the three phases are symmetric (as, e.g., for the model represented by the histogram in Fig.2),

$$m_1^\alpha = m_2^\beta = m_3^\gamma, \quad m_2^\alpha = m_3^\alpha = m_1^\beta = m_3^\beta = m_1^\gamma = m_2^\gamma,$$

but this may not be the case in general.

Suppose the system is in some pure phase o_1 $(o_1 = \alpha, \beta, \gamma)$. According to the thermodynamic theory of equilibrium fluctuations,[51] the probability distribution of homogeneous fluctuations of order parameters m_1, m_2 is

$$\begin{aligned} p(m_1, m_2) &= \sqrt{\det(\kappa)} \frac{V}{2\pi kT/\rho} \exp\left[-\frac{V}{2kT/\rho} (\kappa_{11}(m_1 - m_1^o)^2 \right. \\ &+ \left. 2\kappa_{12}(m_1 - m_1^o)(m_2 - m_2^o) + \kappa_{22}(m_2 - m_2^o)^2) \right], \end{aligned} \tag{7}$$

where $V = L^d$ is the volume of the system. In a semigrand canonical ensemble (SGCE), which we will use for our MC simulations, κ is a 2×2 diagonal matrix with elements

$$\kappa_{ij} = \left(\frac{\partial m_i}{\partial \Delta\mu_j} \right)_{NVT\Delta\mu'} \tag{8}$$

with $\Delta\mu_i = \mu_i - \mu_3$ $(i = 1, 2)$ and μ_i the chemical potential of component i. The prime in eq.(8) indicates that one of the $\Delta\mu$'s is kept constant in the partial derivative. The choice of SGCE is the matter of convenience and efficiency of MC simulations of phase separation in dense fluids[52–54] (see subsection 4.2 for more details). Note that, in the thermodynamic limit, SGCE simulation at fixed $V, T, N, \Delta\mu_1, \Delta\mu_2$ is

equivalent to grand canonical simulation at fixed V, T, and such μ_1, μ_2, μ_3 (fixed) that $\bar{N}$, the grand-canonical average number of molecules in the system, is equal to N.

As clear from eq.(7), the probability of a homogeneous state with one or both order parameters having their intermediate values, $m_{1\text{min}} = (m_1^\alpha + m_1^\gamma)/2$ and $m_{2\text{min}} = (m_2^\beta + m_2^\gamma)/2$, decreases exponentially with the system volume. Hence, for large enough volumes, "homophase" fluctuations with $m_1 = m_{1\text{min}}$ or/and $m_2 = m_{2\text{min}}$ are negligible compared with "heterophase" fluctuations. To show this, we will consider the system (to be simulated) that has the form of a cylinder of length L and radius R (Figure 3). Such a shape will be most convenient (but not necessary) to determine the line tension by computer simulations, but otherwise it does not affect measurable physical quantities because they are obtained by finite-size scaling,[18,19,31,53–55] which involves their extrapolation to infinite cell sizes.

3.1 Determination of the surface tension

For "heterophase" fluctuations, intermediate points on the lines ($\alpha\beta$), ($\beta\gamma$), and ($\gamma\alpha$) in Figure 2b represent the two-phase states of the system with none of the third equilibrium phase present. For example, for a point on the line ($\alpha\beta$) phases α and β coexist while the amount of phase γ is 0, although thermodynamically it can coexist with the α and β. The middle points $o_{\alpha\beta} = \{m_{1\text{min}}, m_{2\text{min}}\}$, $o_{\beta\gamma} = \{m_1^\gamma, m_{2\text{min}}\}$, and $o_{\alpha\gamma} = \{m_{1\text{min}}, m_2^\gamma\}$ on these three lines correspond to the situations when one half of the system is in one phase and the other half in another phase. For example, the point $o_{\alpha\beta}$ corresponds to such s situation that one half of the system is in phase α and the other half in phase β, while the equilibrium phase γ is not present at all. Let us use the generic symbol o_2 to denote the points $o_{\alpha\beta}, o_{\beta\gamma}, o_{\gamma\alpha}$. The difference between the free energies of the system in states o_1 and o_2 is due only to an interfacial contribution F_s from the interface between two coexisting phases in the state o_2. According to the principles of equilibrium thermodynamics, $p(o_2)$ and

$p(o_1)$, the probability densities of two-phase states o_2 and pure phase states o_1, are related as

$$p(o_2) = p(o_1)e^{-F_s/kT}. \tag{9}$$

(phase o_1 is one of two phases in the state o_2)

There is no exact analog of PBC for simulations in a cylindrical geometry, but there are other boundary conditions attenuating the effect of cell boundaries. This issue will be discussed in section 4, but for now it need only be noted that one can impose PBC along the cylinder axis (hereafter called the z-axis) and assume that the effects of the lateral cell boundaries can be neglected. Because of PBC along the z-axis, there may be only three principally different "half-and-half" spatial distributions of two equilibrium phases in the cylinder (Figure 3). Comparing the interfacial free energy contributions F_s in these three cases, one can show that if the aspect ratio $\omega \equiv L/R$ of the cylinder satisfies the inequalities

$$1 < \omega < \pi, \tag{10}$$

then the phase partitioning shown in Fig.3a is thermodynamically most favorable. Hereafter, this will be referred to as the axial "longitudinal" two-phase (AL2P) partitioning. The aspect ratio $\omega < 1$ favors the "droplet-like" phase partitioning (Fig.3b), while $\omega > \pi$ favors the "transversal" phase partitioning (Fig.3c). For the droplet-like phase partitioning the interfacial tension is assumed to be the same as that of a planar interface. This should be a reasonable assumption for a large enough droplet.

If the histogram is obtained by simulations in a cylinder subject to conditions (10) and PBC along the z-axis, one can represent eq.(9) in the form analogous to eq.(4),

$$p(o_2) = aL^x R^y p(o_1)e^{-(2RL\sigma_{o_2})/kT}. \tag{11}$$

Here, σ_{o_2} is the surface tension of a flat interface in an infinite system, and the pre-exponential factor aL^xR^y (with unknown a, x, y) is due to finite size effects (Goldstone modes, capillary waves, etc[18]) that may con-

tribute to F_s, where the leading term $2RL\sigma_{o_2}$ is larger than finite size corrections by an order of magnitude. From eq.(11) it follows that

$$\frac{1}{2RL}\ln\frac{p(o_1)}{p(o_2)} = \frac{\sigma_{o_2}}{kT} - x\frac{\ln L}{2RL} - y\frac{\ln R}{2RL} - \frac{\ln a}{2RL}. \tag{12}$$

Again, for an infinitely large system the RHS of this equation will equal the interfacial tension. The limit $L \to \infty,\ R \to \infty$ can be reached in such a way that $\omega(= L/R)$ remains constant, so that equation (12) can be rewritten in two forms,

$$\begin{aligned} \frac{1}{2RL}\ln\frac{p(o_1)}{p(o_2)} &= \frac{\sigma_{o_2}}{kT} + b\frac{\ln L}{L^2} + c\frac{1}{L^2} \\ &= \frac{\sigma^{o_2}}{kT} + d\frac{\ln R}{R^2} + f\frac{1}{R^2} \end{aligned} \tag{13}$$

with unknown b, c, d, f. The probability distribution as a function of the order parameters, $p(m_1, m_2)$, can be obtained for a series of L's (or R's) via appropriate MC simulations. Then, one can plot the LHS of eq.(13) vs $\ln L/L^2$ (or vs $\ln R/R^2$) and the ordinate intercept of this plot will provide the ratio σ_{o_2}/kT for the interfacial tension in an infinite system.

3.2 Determination of the line tension

"Heterophase" states, corresponding to points lying off the two-phase lines ($\alpha\beta$), ($\beta\gamma$), and ($\gamma\alpha$) in Figure 2b, represent three-phase states such that all three equilibrium phases are simultaneously present in the system. The amount of each phase present is determined by the coordinates of a point o_3' corresponding to a given three-phase state. When the three equilibrium phases are symmetric, the central point e_3 of the composition triangle corresponds to a state in which all three phases are present in equal volumes. In a general case this three-phase volume equi-partition point is not necessarily in the middle of the composition triangle.

Since the subject of the present work is the line tension, we restrict our interest to three-phase equilibria involving three-phase contact regions. The necessary and sufficient condition that there exists such a region

in a three-phase system is

$$\sigma_{\alpha\gamma} < \sigma_{\alpha\beta} + \sigma_{\beta\gamma}, \tag{14}$$

(hereafter double Greek subscripts and superscripts indicate quantities for corresponding two-phase interfaces). Condition (14) means that it is thermodynamically unfavorable for the system to have three phases arranged in three layers parallel to each other. When this condition is fulfilled, F_{sL}, the difference between the free energies of the system in states o_1 and o_3' may contain not only interfacial contributions from three two-phase interfaces, but also the "line tension" contribution from the three-phase contact region. Thus, $p(o_3')$ and $p(o_1)$, the probability densities of three-phase states o_3' and pure phase states o_1 are related as

$$p(o_3') = p(o_1)e^{-F_{sL}/kT}, \tag{15}$$

where the excess free energy F_{sL} has the form

$$F_{sL} = \sigma_{\alpha\beta}A^{\alpha\beta} + \sigma_{\beta\gamma}A^{\beta\gamma} + \sigma_{\alpha\gamma}A^{\alpha\gamma} + \tau L^{\alpha\beta\gamma}. \tag{16}$$

Here the A's are the surface areas of interfaces and $L^{\alpha\beta\gamma}$ is the length of the three phase contact line (assumed to be straight) with which the line tension τ is associated.

Again consider a cylindrical simulation cell with the boundary conditions discussed above, and assume that there exists $1 < \omega_0 < \pi$ such that if $L/R = \omega_0$, then thermodynamically the most favorable three-phase partitioning is the "longitudinal" one shown in Figure 4a. When the three-phase contact line coincides with the axis of the cylinder (as shown in Fig.4a), this will be referred to as the axial longitudinal three-phase (AL3P) partitioning. Denoting by o_3 the corresponding point in the plane m_1, m_2, one can rewrite eq.(15) in the form

$$p(o_3) = aL^x R^y p(o_1)e^{-[(\sigma_{\alpha\beta}+\sigma_{\beta\gamma}+\sigma_{\alpha\gamma})LR+\tau L]/kT}, \tag{17}$$

where now σ's and τ are the interfacial and line tensions, respectively, in an infinite systems, and the pre-exponential factor aL^xR^y (with unknown a, x, y, in general different from those in eq.(11)) is again due to

finite size effects: because σ's and τ in eqs.(16) and (17) are those of an infinitely large system, there may arise small (in comparison with the leading terms) finite-size corrections to F_{sL}.

Henceforth assuming that the simulations are carried out under such conditions that the AL2P and AL3P partitionings are thermodynamically most favorable, one can combine eqs.(11) and (17) and obtain

$$p(o_3) = aL^x R^y [p(o_1)]^{1-\xi} [p(o_2)]^{\xi} e^{-\tau L/kT}, \tag{18}$$

where a, x, y are unknown (different from those in eqs.(11) and (17)) and

$$\xi = \frac{\sigma_{\alpha\beta} + \sigma_{\beta\gamma} + \sigma_{\alpha\gamma}}{2\sigma_{o_2}}. \tag{19}$$

From eq.(18) it follows that

$$\frac{1}{L} \ln \frac{[p(o_2)]^{\xi}}{[p(o_1)]^{\xi-1} p(o_3)} = \frac{\tau}{kT} - x\frac{\ln L}{L} - y\frac{\ln R}{L} - \frac{\ln a}{L}. \tag{20}$$

For an infinitely large system the RHS of eq.(20) will equal the ratio of the line tension τ to kT. If the limit $L \to \infty,\ R \to \infty$ is reached in such a way that $\omega \equiv L/R$ remains constant, then eq.(20) can be rewritten as

$$\begin{aligned} \frac{1}{L} \ln \frac{[p(o_2)]^{\xi}}{[p(o_1)]^{\xi-1} p(o_3)} &= \frac{\tau}{kT} + b\frac{\ln L}{L} + c\frac{1}{L} \\ &= \frac{\tau}{kT} + d\frac{\ln R}{R} + f\frac{1}{R} \end{aligned} \tag{21}$$

with unknown b, c, d, f. Again, $p(m_1, m_2)$, the probability distribution as a function of the order parameters, can be obtained for a series of L's (or R's) via appropriate Monte-Carlo simulations at constant $\omega(= L/R)$. Then, one can plot the LHS of eq.(19) vs $\ln L/L$ (or vs $\ln R/R$) and the ordinate intercept of this plot will provide the ratio τ/kT for the line tension in the infinite system.

It is worth emphasizing that the point o_1 in eqs.(9)-(21) corresponds to any pure phase state (α, β, or γ) because (ideally) in a three-phase equilibrium $p(m_1^{\alpha}, m_2^{\alpha}) = p(m_1^{\beta}, m_2^{\beta}) = p(m_1^{\gamma}, m_2^{\gamma})$. The point o_2 represents any two-phase equilibrium with the AL2P partitioning (Fig.3a) involving o_1 phase, and σ_{o_2} in

eqs.(11)-(13),(19) is the corresponding interfacial tension. Finally, the point o_3 in eqs.(17)-(21) represents the AL3P partitioning (Fig.4a).

4 General set-up of the simulation cell and boundary conditions

For simulations in a rectangular geometry one usually uses PBC in order to decrease the effect from the simulation cell boundaries. For simulations in a cylindrical geometry, there is no exact analog of PBS, but one can impose boundary conditions that do attenuate the effect of cell boundaries. Namely, one can impose the usual PBC along the z-axis (Figures 3 and 4). In the plane of polar coordinates ϕ, r, perpendicular to the z-axis, impose "random-periodic" boundary conditions (RPBC); that is, if upon an elementary Monte-Carlo move the *new* coordinates z, ϕ, r of a molecule are such that $r > R$ (i.e., the molecule crosses through the lateral surface of the cylinder), the angle ϕ is replaced by a new, *random* angle ϕ' and the radius r is replaced by a new, *periodic* value $r' = R - (r - R)$. After these changes are made, the acceptance criterion is checked and the move is either accepted or rejected. If the move is rejected, the molecule keeps its old coordinates (those prior to generating new coordinates z, ϕ, r). In this work only hard-sphere type molecular interactions are considered, but in a general case (e.g., Lennard-Jones intermolecular potential) it would be necessary to deal with the problem of accounting for the interactions of "random-periodic" images of molecules, that are in the lateral surface layer of "cutoff" thickness, with other molecules in this layer.

The propensity of an equilibrium system to minimize its free energy and PBC along the z-axis prevent the formation of artificial (i.e., due to the finite size of the simulation cell) phase interfaces at the bases of the cylinder. However, imposing RPBC in the ϕ, r plane gives rise to the *probabilistic* phase interfaces at the lateral surface of the cylinder. Actually, with RPBC imposed, a molecule crossing the lateral interface will

leave phase s_1 and enter phase s_2 with the probability $g_{s_1 s_2}$ ($s_1, s_2 = \alpha, \beta, \gamma$),

$$g_{s_1 s_2} = g_{s_2 s_1} = \frac{s_1 s_2}{(2\pi)^2} \qquad (s_1, s_2 = \alpha, \beta, \gamma), \tag{22}$$

(where s_1 and s_2 are not subscripts, they must be understood as the corresponding contact angles) with the normalization condition $\sum g_{s_1 s_2} = 1$ naturally satisfied. Thus, the whole lateral surface of area $2\pi RL$ is an $\alpha\beta$ interface with the probability $2g_{\alpha\beta}$, a $\beta\gamma$ interface with the probability $2g_{\beta\gamma}$, and an $\alpha\gamma$ interface with the probability $2g_{\alpha\gamma}$. Clearly, for any point o_2 (half-and-half two-phase coexistence) the analogous probability is $2g_{o_2} = 1/2$.

Thus, as an artifact of RPBC imposed at the lateral surface of the simulation cell (cylinder), it is necessary to modify equations (11)-(13), (17), and (19). Namely, eqs.(11)-(13) must be replaced by

$$p(o_2) = aL^x R^y p(o_1) e^{-(2+\pi)RL\sigma_{o_2}/kT}, \tag{23}$$

$$\frac{1}{(2+\pi)RL} \ln \frac{p(o_1)}{p(o_2)} = \frac{\sigma_{o_2}}{kT} - x\frac{\ln L}{(2+\pi)RL} - y\frac{\ln R}{(2+\pi)RL} - \frac{\ln a}{(2+\pi)RL}, \tag{24}$$

$$\begin{aligned} \frac{1}{(2+\pi)RL} \ln \frac{p(o_1)}{p(o_2)} &= \frac{\sigma^{o_2}}{kT} + b\frac{\ln L}{L^2} + c\frac{1}{L^2} \\ &= \frac{\sigma_{o_2}}{kT} + d\frac{\ln R}{R^2} + f\frac{\ln R}{R^2}, \end{aligned} \tag{25}$$

respectively. Equations (17) and (19) must be replaced by

$$p(o_3) = aL^x R^y p(o_1) e^{-[((1+4\pi g_{\alpha\beta})\sigma^{\alpha\beta} + (1+4\pi g_{\beta\gamma})\sigma_{\beta\gamma} + (1+4\pi g_{\alpha\gamma})\sigma^{\alpha\gamma})LR + \tau L]/kT}, \tag{26}$$

$$\xi = \frac{(1+4\pi g_{\alpha\beta})\sigma_{\alpha\beta} + (1+4\pi g_{\beta\gamma})\sigma_{\beta\gamma} + (1+4\pi g_{\alpha\gamma})\sigma_{\alpha\gamma}}{(2+\pi)\sigma_{o_2}}. \tag{27}$$

Now, the ratio σ_{o_2}/kT for the surface tension of an infinite system is determined as the ordinate intercept of the plot of the LHS side of eq.(25) vs $\ln L/L^2$ (or vs $\ln R/R^2$). The ratio τ/kT for the line tension in an infinite system is found, as previously, by plotting the LHS of eq.(21) vs $\ln L/L$ (or vs $\ln R/R$) and finding the ordinate intercept of this plot, but the parameter ξ is now given by eq.(27) rather than eq.(19).

Note that even with perfect PBC imposed on the finite simulation cell, there may be cell *boundary* contributions to F_s and F_{sL}, but they can be expected to be much smaller than the above contributions from the *physical* phase interfaces at the cell boundaries. Moreover, in the case where the equilibrium phases are symmetric (such as Ising-like models, the model discussed below, etc), the cell *boundary* contributions to F_s (and F_{sL}) can be assumed to be zero[18,55] because in such systems the free energy of the cell is affected by its boundaries in the same way, independently of which phases are present.

4.1 Method specifics for the simulated model

To illustrate the proposed method with a concrete example, MC simulations were carried out for the three-dimensional three-component fluid mixture, in which the molecules of different species interact as hard spheres, whereas molecules of the same species do not interact at all (i.e., are completely penetrable by one another).[47−49] This is a natural generalization of the binary model, earlier proposed by Widom and Rowlinson[56] and come to be known as the primitive version of the Widom-Rowlinson model. The intermolecular potentials between two molecules of species i and j at a distance r from each other are defined as

$$u_{ii}(r) = 0 \quad (i = 1, 2, 3), \tag{28}$$

$$u_{ij}(r) = 0 \quad (r > \eta, i \neq j = 1, 2, 3), \qquad u_{ij}(r) = \infty \quad (r < \eta, i \neq j = 1, 2, 3), \tag{29}$$

so that the molecules of each pure species constitute an ideal gas, while every molecule of species i sees every molecule of species $j \quad (j \neq i)$ as a hard sphere of diameter η. The phase behavior of this system was analytically studied in both mean-field and higher order approximations.[47−49] The system is predicted to have a so-called "quadruple point" density ρ_q: at this density within the composition triangle there is a smaller one (similar to and co-centered with the former) where an equimolar ternary mixture may exist in equilibrium with three symmetric phases each rich in one of three components. When the density becomes

greater than ρ^q, the equimolar phase is no longer present and the inner four-phase triangle becomes a three-phase coexistence region. The three coexisting phases α, β, and γ are related symmetrically: phase α is rich in component 1 with equal traces of 2 and 3, phase β is rich in 2 with equal traces of 1 and 3, and phase γ is rich in 3 with equal traces of 1 and 2.

Since the three coexisting phases α, β, and γ are absolutely symmetric, the three interfacial tensions are all equal, $\sigma^{\alpha\beta} = \sigma^{\beta\gamma} = \sigma^{\alpha\gamma} = \sigma$. Therefore a three-phase coexistence will necessarily involve a three phase contact region with the contact angles $\alpha = \beta = \gamma = 2\pi/3$. Furthermore, for the appropriate size and aspect ratio ω_0 of the cylindrical simulation cell, the point o_3 which corresponds to the AL3P partitioning will coincide with the phase volume equi-partition point e_3, and both o_3 and e_3 lie exactly in the center of the three-phase triangle.

As an alternative to AL3P, the three-phase partitioning may be of mixed character as illustrated in Fig.4b (for $\omega > \omega' = (6 - 8/\pi)/\sqrt{3}$) and Fig.4 (for $\omega < \omega'$). Knowing the contact angles ($\alpha = \beta = \gamma = 2\pi/3$) enables one to determine the conditions under which in the state e_3 (=o_3) the AL3P partitioning (Fig.4a) is thermodynamically most favorable:

$$\frac{s(\omega)}{4-\omega} > -\frac{\tau}{\sigma R} \quad (1 < \omega \leq \pi), \tag{30}$$

(only the range $1 < \omega < \pi$ is considered because of condition (10) for the AL2P partitioning). The explicit form of the continuous function $s(\omega)$ is given in the Appendix. The function $s(\omega)/(4-\omega)$ is positive for $1 < \omega < \omega^* \simeq 2.465$, attaining its maximum at $\omega \simeq 1.635$. Thus, if $\tau > 0$ and $1 < \omega \lesssim \omega^*$, the AL3P partitioning (shown in Fig.4a) is thermodynamically more favorable than those in Fig.4b and Fig.4c. When $\tau < 0$ (as the mean-field theory predicts[36] for the 3d3c-PS model) and $1 < \omega \lesssim \omega^*$, making the AL3P partitioning thermodynamically most favorable requires that R be sufficiently large,

$$R > R^* = \frac{4-\omega}{s(\omega)} \frac{|\tau|}{\sigma}.$$

Evaluating R^* accurately prior to simulations is complicated by the absence of data on τ, even though data on σ were readily available. Besides, taking large R's (for a given density) leads to a significant increase in the CPU time for MC simulations. If this is not an acceptable option, one can use a modified version of the above method. For the case of a mixed three-phase partitioning, the modifications lead to the equations

$$p(o_3) = aR^x[p(o_1)]^{1-\xi}[p(o_2)]^{\xi}e^{-4R\tau/kT}, \tag{31}$$

$$\xi = \frac{\phi(\omega)}{(2+\pi)\omega}, \tag{32}$$

$$\begin{aligned} \frac{1}{4R}\ln\frac{[p(o_2)]^{\xi}}{[p(o_1)]^{\xi-1}p(o_3)} &= \frac{\tau}{kT} + b\frac{\ln R}{R} + c\frac{1}{R} \\ & \frac{\tau}{kT} + d\frac{\ln L}{L} + f\frac{1}{L} \end{aligned} \tag{33}$$

where a, x, b, c, d, f are unknown and the explicit form of the function $\phi(\omega)$ is given in the Appendix. Generating $p(m_1, m_2)$, the probability distribution as a function of the order parameters, via appropriate MC simulations for a series of R's (or L's) at constant $\omega = L/R$, and plotting the LHS of eq.(33) vs $\ln R/R$ (or $\ln L/L$), one finds the ratio τ/kT as the ordinate intercept of this plot.

4.2 Monte-Carlo procedure and results

To obtain the histogram of a system showing a demixing phase transition, most convenient are SGCE MC simulations[57–59], where it is necessary to explore all configurations and compositions of the system for a constant total number of molecules. The configurational space is sampled as in a standard canonical simulation. Varying the composition is carried out by the so-called "identity change" MC moves, and can be done in two different ways: (1) choose a molecule at random, change its identity, and accept or reject the change; (2) choose a component at random, choose a molecule of that component at random, change its identity, and accept or reject the change. These two methods of composition sampling correspond to two different ways

to express the SGCE partition function.[57] As a consequence, the acceptance criteria for these methods are different. As a slight modification of this algorithm, an identity change attempt may be combined with the configurational displacement of a molecule.[60,61] The choice between a pure spatial MC displacement and a combined "spatial displacement+identity change" MC move is uniformly random.

The most obvious advantage of SGCE MC simulations over the Gibbs ensemble simulations[63−65] is that less computational effort is required by the former (single phase simulations of N particles) compared to the latter (two-phase simulation of $N + N$ molecules). Besides, the Gibbs ensemble method relies on particle transfers from one fluid phase (=simulation box) into another, which gives rise to technical limitations when studying relatively dense phases, because the probability of particle insertion is then very low and the method becomes inefficient. Similar and other problems arise in a grand canonical ensemble simulations of dense fluids, although recently some special techniques have been developed to overcome or alleviate those problems[23,30,31,51,55]

As a test of the simulation algorithm, the SGCE MC simulations were carried out for the primitive version of the two-dimensional Widom-Rowlinson model[56] in a square cell with standard PBC and the critical density was determined by using the method proposed by Binder and co-workers.[19,52,53,62] They showed that for demixing phase transitions in two-component mixtures, the ratio $< s^2 > / < |s| >^2$ (the reduced second moment of $s = 2m - 1$, with m being the order parameter) at the critical density ρ_c is independent of the system size. Hence, ρ_c in such systems can be determined as the density at which the curves "$< s^2 > / < |s| >^2$ vs density" for different system sizes cross. The simulations were carried out for four different total numbers of molecules in the system: $N = 256,\ 726,\ 1024$, and 4098. The results are shown in Figure 5, where $< s^2 > / < |s| >^2$ is plotted as a function of the dimensionless density $\rho\eta^2$ for four N's. The critical density was determined as the average of six densities at which six pairs of simulated series cross. The standard deviation of this scatter dominates the standard deviation of $< s^2 > / < |s| >^2$ for any given

density in a single simulation run. Thus for a two-dimensional Widom-Rowlinson model the dimensionless critical density was found to be $\rho_c\eta^2 \simeq 1.58 \pm 0.01$. This is very close to the result reported previously by Johnson et al.,[66] who used the invaded cluster (IC) approach in MC simulations: $\rho_c\eta^2 \simeq 1.566 \pm 0.003$. To our knowledge, there have been no other simulations of this model so far.

The MC simulations of the three-component three-dimensional model were carried out in a cylindrical cell with PBC along the z-axis and RPBC at the lateral surface of the cell. Two densities, $\rho\eta^3 = 0.83$ and $\rho\eta^3 = 0.85$, were considered, both slightly higher than the quadruple point density of this model reported previously[66] as $\rho_q\eta^3 \simeq 0.796$. A series of histograms were obtained for each density by carrying out simulations for different cylinder sizes L (and R, with $\omega = L/R = const = 1.5$). Equation (25) was then applied to each series and the surface tension σ for an infinite system was found by extrapolating the series to $\ln R/R^2 \to 0$ (see Figure 6): $\sigma\eta^2/kT = 0.0037 \pm 0.0005$ for $\rho\eta^3 = 0.83$, and $\sigma\eta^2/kT = 0.0063 \pm 0.0008$ for $\rho\eta^3 = 0.85$. As expected, the surface tension increases with increasing density as the three phases become less and less miscible. Furthermore, according to the mean field approximation,[36] the line tension in this model above the quadruple point density is expected to be negative. Hence, prior to obtaining the final result, there is some uncertainty whether condition (30) is fulfilled for a given R (with $\omega = 1.5$). The line tension was thus determined by using both eq.(21) and eq.(33) and the results were substituted into eq.(30) for verification. In neither case condition (30) held whence one can conclude that the dominant three-phase partitioning is the one shown in Fig.4b, and eq.(33) is the appropriate one for determining the line tension. The results for both densities (as shown in Figure 7) are: $\tau\eta/kT = -0.093 \pm 0.006$ for $\rho\eta^3 = 0.83$ and $\tau\eta/kT = -0.103 \pm 0.008$ for $\rho\eta^3 = 0.85$. As expected,[36] the line tension is negative. Relatively large standard deviations (about 10% of average values) of results for σ/kT and τ/kT are due to the uncertainty in finding the probabilities $p(o_1),\ p(o_2)$, and $p(o_3)$ from a simulated histogram. To increase the accuracy of simulated σ/kT and τ/kT, simulations longer than 2×10^7 MC sweeps (a typical length of one simulation

run in the present work) are required.

5 Conclusions

A system where the three-phase equilibrium involves a three-phase contact region has been studied. The main thermodynamic characteristic of a three-phase contact region is the line tension, defined as the linear excess grand canonical potential per unit length of the contact line. In such a system, the probability distribution of states of the system with respect to two independent order parameters depends on both the surface and line tensions. This constitutes the foundation of a method for determining the line tension by MC simulations (either in a semi-grand canonical, or in a grand canonical or in a Gibbs ensemble) proposed in the present work. The method is the combination of the analysis of the probability distribution function and finite-size scaling, and is the natural development of Binder's approach[18] to studying interfacial phenomena and phase equilibria in two-phase systems. MC simulations allow one to obtain the probability distribution of states of the system as a normalized histogram. However, the histogram provided by MC simulations and results extracted therefrom depend on the size of the simulated system. Carrying out simulations for a series of system sizes, and extrapolating the results obtained from the corresponding series of histograms to the infinite size, one can determine the line tension of the three-phase contact region and the interfacial tensions of all three interfaces in an infinite system (and hence the contact angles). The proposed method is illustrated by its application to the three-dimensional ternary fluid mixture, in which molecular pairs of like species do not interact whereas those of unlike species interact as hard spheres. The three-phase equilibrium in this model above its quadruple-point density involves a three-phase contact region. As expected, the interfacial tension increases with increasing density. The behavior of the line tension is also compatible with what one would expect based on the mean-field approximation,[36] although the predictions of the latter must be

regarded with caution because of the large discrepancy between the mean-field quadruple point density[47,48] ($\rho_q^{\rm MF}\eta^3 \simeq 0.601$) and the simulated one[66] ($\rho_q^{\rm MC}\eta^3 \simeq 0.796$).

The present work suggests that the most accurate data for the line tension can be obtained by simulations in a cylindrical cell under conditions where there is only one three-phase contact line in the cell. For a positive line tension this condition can be easily fulfilled by an appropriate choice of the aspect ratio of the cylinder. For a negative line tension this condition may require the cylinder to have not only a suitable aspect ratio but also a large enough radius which may lead to a drastic increase of simulation time. In this case it may be a better choice to conduct simulations under conditions where there are two three-phase contact lines in the simulation cell. However, in this case the accuracy of results for the line tension can suffer if the contact lines are so close that the inhomogeneities in two three-phase contact regions overlap. In order to avoid this effect it is necessary to take longer cylinders which again leads to an increase in simulation time.

It follows from the foregoing that it is possible to determine the line tension by simulations in a cubic cell with PBC in two directions, say x and y, and anti-PBC in the third, say z (the extension of our method to this case will be given in a sequel[67] to the present work). Moreover, combining such simulations with the canonical ensemble MC simulations, carried out under the same boundary conditions and appropriate choice of the order parameters, makes it possible to verify the validity of the new linear adsorption equation[39] $d\tau = -\sum_i \Lambda_i \Delta\mu_i + c_\alpha d\alpha + c_\beta d\beta + c_\gamma d\gamma$, where $d\tau$ is the change in the line tension due to the changes $d\mu_i \quad (i = 1, 2, 3)$ of the field variables μ_i and Λ_i is the linear adsorption of component i. The last three terms ($c_\alpha d\alpha$, etc) on the RHS of the above equation make a difference between the old[2,19] and modified[39] versions of the linear adsorption equation. At present, there are no recipes to analytically evaluate the coefficients $c_\alpha, c_\beta, c_\gamma$. However, the proposed method enables one to find $d\tau$, while the subsequent canonical MC simulations can provide $\sum_i \Lambda_i d\mu_i$. The inequality $d\tau + \sum_i \Lambda_i \Delta\mu_i \neq 0$ could be regarded as an indirect "simulational" confirmation of the validity of the modified linear adsorption equation (this will also be

discussed in the sequel.[67]). Recently,[40] this inequality was shown to hold in the framework of the square-gradient approximation of density-functional theory with a special choice for the local part of the free-energy density. Note that in the model system, simulated in the present work, $d\alpha = d\beta = d\gamma = 0$ for any changes of field variables. Thus, in this particular model $d\tau = -\sum_i \Lambda_i \Delta\mu_i$, so another model is needed to simulate the validity of the new linear adsorption equation.

Finally, it should be noted that the proposed method can be easily modified to study wetting phenomena and, in particular, to determine the line tension attributed to the region of contact of two equilibrium fluid phases with an "inert" rigid substrate. As in the case of two-phase equilibrium discussed in section 2, the probability distribution of states of such a system is a function of only one independent order parameter, but the two maxima of this function (histogram) will now depend on the corresponding fluid-substrate interfacial tensions and hence may not be equal, unlike the situation described in section 2 and Figure 1. Furthermore, the minimum of this function will now depend on the line tension associated with the "fluid-fluid-substrate" contact region and may not be located strictly in the middle between the two maxima. A statistical-mechanical basis for determining the line tension in such a system by MC simulations will be given in a sequel[67] to the present work.

Acknowledgements

The author is grateful to B. Widom for many helpful discussions and reading the manuscript of this work, which was done as a part of Widom's research program at Cornell University. It was supported by the U.S. National Science Foundation and the Cornell Center for Material Research.

Appendix. Explicit form of auxiliary functions $s(\omega)$ and $\phi(\omega)$

The function $s(\omega)$ in inequality (30) is defined as

$$\begin{aligned} s(\omega) &= -\frac{1}{3}(3+\pi)\omega + \frac{6}{\sqrt{3}}\pi - \frac{4}{\sqrt{3}}g(\omega) - \frac{12}{\sqrt{3}}\arccos g(\omega) \\ &\quad + \frac{8}{\sqrt{3}}g(\omega)\sqrt{a-g^2(\omega)} - \frac{3}{2\sqrt{3}\pi g(\omega)}[\pi - 2\arccos g(\omega)]^2 \quad (1<\omega\leq\omega'), \end{aligned} \tag{A1}$$

$$s(\omega) = -\frac{1}{3}(5+2\pi) + \frac{13}{2\sqrt{3}}\pi - \frac{8}{3\sqrt{3}} - \frac{16}{3\sqrt{3}\pi} \quad (\omega'<\omega<\pi), \tag{A2}$$

where $g(\omega)$ is the solution of the equation

$$\frac{3}{4}\pi g(\omega) + \frac{1}{2}(1-g(\omega))Q(g(\omega)) = \frac{\sqrt{3}}{4}\pi\omega + 1 \tag{A3}$$

with the function $Q(x)$ of some variable x being defined as

$$Q(x) = \frac{3\sin\arccos x - 3x\arccos x - 3\sin^3\arccos x}{1-x}. \tag{A4}$$

The function $\phi(\omega)$ in eq.(32) is defined as

$$\begin{aligned} \phi(\omega) &= (2+\pi)\omega + \frac{6}{\sqrt{3}}\pi - \frac{4}{\sqrt{3}}g(\omega) - \frac{1}{2}\sqrt{3}\arccos g(\omega) \\ &\quad + \frac{8}{\sqrt{3}}g(\omega)\sqrt{a-g^2(\omega)} - \frac{3}{2\sqrt{3}\pi g(\omega)}[\pi - 2\arccos g(\omega)]^2 \quad (1<\omega\leq\omega'), \end{aligned} \tag{A5}$$

$$\phi(\omega) = \frac{2}{3}(2+\pi) + \frac{13}{2\sqrt{3}}\pi - \frac{8}{3\sqrt{3}} - \frac{16}{3\sqrt{3}\pi} \quad (\omega'<\omega<\pi), \tag{A6}$$

with $g(\omega)$ defined by eq.(A3).

References

[1] J. G. Kirkwood and F. P. Buff, J. Chem. Phys. 17, 338 (1949).

[2] J.S. Rowlinson and B. Widom, *Molecular Theory of Capillarity* (Clarendon Press, Oxford, 1982).

[3] R. Evans, Adv.Phys. **28**, 143 (1979).

[3] R. Evans, *Fundamentals of inhomogeneous fluids*, edited by D. Henderson (Marcel Dekker, NY, 1992), pp.85-175.

[5] B. Widom, *Phase Transitions and Critical Phenomena*, edited by C. Domb and M.S. Green (Academic, New York, 1972), vol.II, pp.79-100.

[6] F.P. Buff, R.A. Lovett, and F.H. Stillinger,Jr., Phys. Ref. Lett. **15**, 621 (1965).

[7] J. K. Lee, J. A. Barker, and G. M. Pound, J. Chem. Phys. **60**, 1976 (1974).

[8] M. J. P. Nijmeijer, A. F. Bakker, C. Bruin, and J. H. Sikkenk, J. Chem. Phys. **89**, 3789 (1988).

[9]J. A. Barker, Mol. Phys. **80**, 815 (1993).

[10]C. D. Holcomb, P. Clancy, and J. A. Zollweg, Mol. Phys. **78**, 437 (1993).

[11]J. Miyazaki, J. A. Barker, and G. M. Pound, J. Chem. Phys. **64**, 3364 (1976).

[12]E. Salomons and M. Mareschal, J. Phys. Condensed Matter **3**, 3645 (1991).

[13]J. Potvin and C. Rebbi, Phys. Rev. Lett. **62**, 3062 (1989).

[14]H. Gausterer, J. Potvin, C. Rebbi, and S. Sanielevici, Physica A **192**, 525 (1993).

[15]J. E. Hunter III, W. P. Reinhardt, and T. F. Davis, J. Chem. Phys. **99**, 6856 (1993).

[16]K. K. Mon and D. Jasnow, Phys. Rev. A **30**, 670 (1984); *ibid.* Phys. Rev. A **31**, 4008 (1985).

[17]M. Hasenbusch, J. Phys. I France **3**, 753 (1993).

[18]K. Binder, Phys. Rev. A **25**, 1699 (1982).

[19]K. K. Mon and K. Binder, J. Chem. Phys. **96**, 6989 (1992).

[20]B. Grossmann and M. L. Laursen, Nucl. Phys. B **408**, 637 (1993).

[21]B. A. Berg, U. Hansmann, and T. Neuhaus, Phys. Rev. B **47**, 497 (1993).

[22]B. A. Berg, U. Hansmann, and T. Neuhaus, Z. Phys. B **90**, 229 (1993).

[23]B. A. Berg and T. Neuhaus, Phys. Rev. Lett. **68**, 9 (1992).

[24]A. Billoire, T. Neuhaus, and B. A. Berg, Nucl. Phys. B **413**, 795 (1994).

[25]W. Janke, B. A. Berg, and M. Katoot, Nucl. Phys. B **382**, 649 (1992).

[26]N. A. Alves, Phys. Rev. D **46**, 3678 (1992).

[27]J .E. Hunter III and W.P. Reinhardt, J. Chem. Phys. **103**, 8627 (1995).

[28]J. J. Potoff and A.Z. Panagiotopoulos, J. Chem. Phys. **112**, 6411 (2000).

[29]J. K. Singh, D.A. Kofke, J.R. Errington, J. Chem. Phys. **119**, 3405 (2003).

[30]P. Virnau, M. Müller, L.G. MacDowell, and K. Binder, J. Chem. Phys. **121**, 2169 (2004).

[31]R. L. C. Vink, J. Horbach, and K. Binder, (submitted to ???, 2004)

[32]D. Platikanov, M. Nedyalkov, and A. Scheludko, J. Colloid Interface Sci. **75**, 612 (1980).

[33]D. Platikanov, M. Nedyalkov, and V. Nasteva, J. Colloid Interface Sci. **75**, 620 (1980).

[34]P.-H. Puech, N. Borghi, E. Karatekin, and F. Brochard-Wyart, Phys.Rev.Lett. **90**, 128304 (2003).

[35]L. Boruvka and A.W. Neumann, J. Chem. Phys. **66**, 5464 (1977).

[36]J. Kerins and B. Widom, J. Chem. Phys. **77**, 2061 (1982).

[37]I. Szleifer and B. Widom, Molec. Phys., **75**, 925 (1992).

[38]B. Widom, Colloids Surf. A **239**, 141 (2004).

[39]Y. Djikaev and B. Widom, J. Chem. Phys. **121**, 5602 (2004).

[40]C. M. Taylor and B. Widom, (accepted for publication in JCP, 2004)

[41]P. Tarazona and G. Navascués, J. Chem. Phys. **75**, 3114 (1981).

[42]M.J.P. Nijmeijer, C. Bruin, A.F. Baker, and J.M.J. Van Leeuwen, Phys. Rev. A **42**, 6052 (1990).

[43]F. Bresme and N. Quirke, J. Chem. Phys. **112**, 5985 (2000); *ibid*. J. Chem. Phys. **110**, 3536 (1999); *ibid*. Phys. Chem. Chem. Phys.**1**, 2149 (1999); *ibid*. Phys. Rev. Lett. **80**, 3791 (1998).

[44]A. Patrykiejew, L. Salamacha, S. Sokoowski, and O. Pizio, Phys. Rev. E **67**, 061603 (2003).

[45]A. Milchev, M. Müller, K. Binder, and D. P. Landau, Phys. Rev. E **68**, 031601 (2003).

[46]D.R. Heine, G.S. Grest, and E. B. Webb III, Phys. Rev. E **70**, 011606 (2004).

[47]M.I. Guerrero, J.S. Rowlinson, and G. Morrison, J. Chem. Soc. Faraday Trans. II **72**, 1970 (1976).

[48]N. Derosier, M.I. Guerrero, J.S. Rowlinson, and D. Stubley, J. Chem. Soc. Faraday Trans. II **73**, 1632 (1977).

[49]J.S.Rowlinson, Adv. Chem. Phys. **41**, 1 (1980).

[50]M. Fitzgerald, R.R. Picard, and R.N. Silver, Europhys. Lett. **46**, 282 (1999).

[51]T. Hill, *Statistical Mechanics* (McGraw-Hill, New York, 1956).

[52]H.-P. Deutsch and K. Binder, Macromolecules **25**, 6214 (1992).

[53]H.-P. Deutsch, J. Stat. Phys. **67**, 1039 (1992).

[54]A. M. Ferrenberg and R. H. Swendsen, Phys. Rev. Lett. **61**, 2635 (1988).

[55]K. Binder, Z. Phys. B **43**, 119 (1981).

[56]B. Widom and J.S. Rowlinson, J. Chem. Phys. **52**, 1670 (1970).

[57]D. A. Kofke and E. D. Glandt, Mol. Phys. **64**, 1105 (1988).

[58]D. Frenkel, *Computer Simulation in Chemical Phsysics*, edited by M.P. ALlen and D.J. Tildesly (Kluwer Academic, New York, 1993), pp.93-152.

[59]E. de Miguel, E.M. del Rio, and M.M. Telo da Gama, J. Chem. Phys. **103**, 6188 (1995).

[60]C.-Y. Shew and A. Yethiraj, J. Chem. Phys. **104**, 7665 (1996).

[61]K. Jagannathan and A. Yethiraj, J. Chem. Phys. **118**, 7907 (2003).

[62]K. Binder, Phys. Rev. Lett. **47**, 693 (1982).

[63]A. Z. Panagiotopoulos, Mol. Phys. **61**, 813 (1987).

[64]A. Z. Panagiotopoulos, Mol. Simul. **9**, 1 (1992).

[65]B. Smit, *Computer Simulation in Chemical Phsysics*, edited by M.P. ALlen and D.J. Tildesly (Kluwer Academic, New York, 1993), pp.173-205.

[66]G. Johnson, H.Gould, J. Machta, and L.K. Chayes, Phys. Rev. Lett. **79**, 2612 (1997).

[67]Y. Djikaev *Manuscript in preparation...*

Captions to Figures 1-7

of the manuscript "HISTOGRAM ANALYSIS AS A METHOD FOR DETERMINING THE LINE TENSION BY MONTE-CARLO SIMULATAIONS" by Yuri Djikaev.

Figure 1: Typical "histogram", probability distribution p of states of a system with respect to a single order parameter m, under conditions of two-phase coexistence. The values of the order parameter in two equilibrium phases are m^α and m^β

Figure 2: Typical probability distribution p of states of a system with respect to two order parameters m_1 and m_2 under conditions of three-phase coexistence, obtained for a three-dimensional ternary fluid mixture, in which molecular pairs of like species do not interact whereas those of unlike species interact as hard spheres, at the total density $\rho\eta^3 = 0.85$. a) Three-dimensional plot; b) Projection of the histogram onto the mole-fraction plane (for details see the text).

Figure 3: Three two-phase (half-and-half) partitionings compatible with the periodic boundary conditions along the z axis: a) AL2P partitioning; b) droplet-like partitioning; c) transversal partitioning.

Figure 4: a) The axial longitudinal three-phase (AL3P) partitioning in the cylindrical simulation cell with the contact angles $\alpha,\ \beta$, and γ; b) and c) - the alternative to AL3P three-phase partitionings in the cilinder for $\omega > \omega'$ and $\omega < \omega'$ respectively

Figure 5: Determination of the critical density for the primitive version of the two-dimensional Widom-Rowlinson model by SGCE MC simulations. The reduced second moment $\langle s^2\rangle/\langle|s|\rangle^2$ ($s = 2m - 1$ with m the mole fraction of one of two components) is plotted vs dimensionless density $\rho\eta^2$ for four different numbers of molecules in the simulated system (square with PBC): larger circles are for $N = 256$, smaller

points for $N = 726$, smaller circles for $N = 1024$, and larger points for $N = 4098$. The thin curves are plotted only for guiding the eye. The dashed vertical line indicates the critical density from ref.66.

Figure 6: Determination of the surface tension by the histogram analysis combined with the finite size scaling. The LHS of eq.(25) is plotted vs $\ln L/L^2$ for two different densities, $\rho\eta^3 = 0.83$ (upper series) and $\rho\eta^3 = 0.85$ (lower series). The straight lines show the linear least-squares fits to each series of simulated points. The extrapolated values for the infinite system size are: $\sigma\eta^2/kT = 0.0037 \pm 0.0005$ for $\rho\eta^3 = 0.83$, and $\sigma\eta^2/kT = 0.0063 \pm 0.0008$ for $\rho\eta^3 = 0.85$.

Figure 7: Determination of the surface tension by the histogram analysis combined with the finite size scaling. The LHS of eq.(33) is plotted vs $\ln L/L$ for two different densities, $\rho\eta^3 = 0.83$ (upper series) and $\rho\eta^3 = 0.85$ (lower series). The straight lines show the linear least-squares fits to each series of simulated points. The extrapolated values for the infinite system size are: $\tau\eta/kT = -0.093 \pm 0.006$ for $rho\eta^3 = 0.83$, and $\tau\eta/kT = -0.103 \pm 0.008$ for $rho\eta^3 = 0.83$.

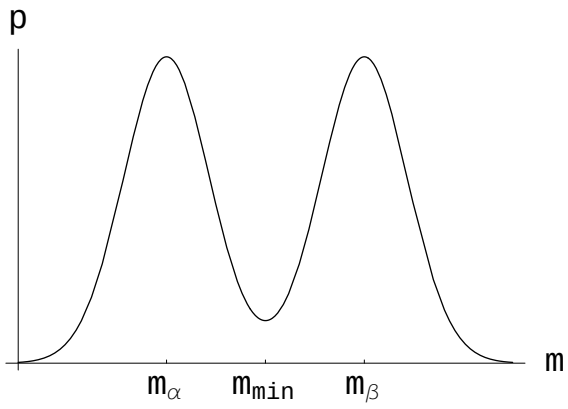

Figure 1:

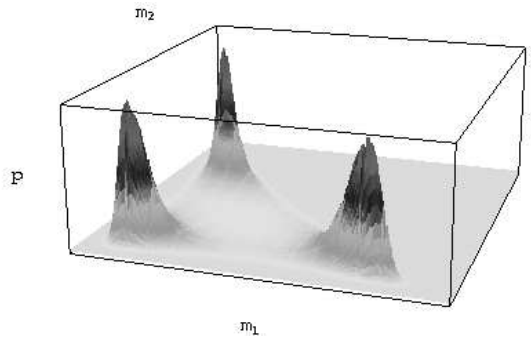
m2
p
m1

a)

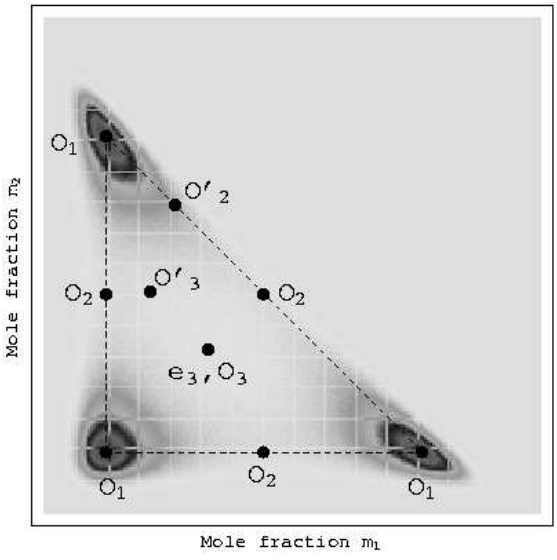
O1
O'2
O'3
O2
O2
e3, O3
O1
O2
O1
Mole fraction m2
Mole fraction m1

b)

Figure 2:

a)

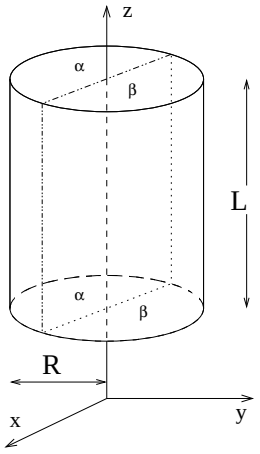

b)

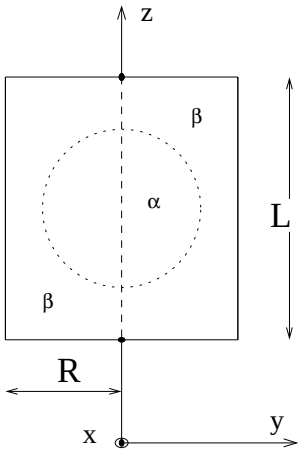

c)

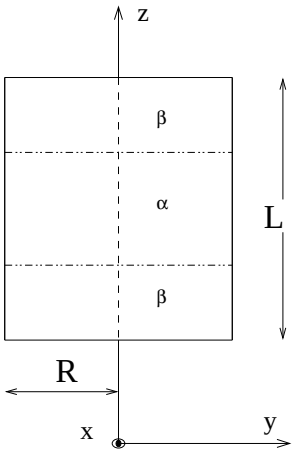

Figure 3:

a)

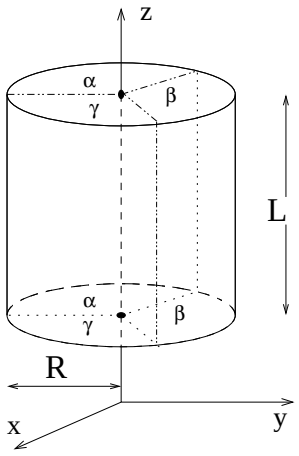

b)

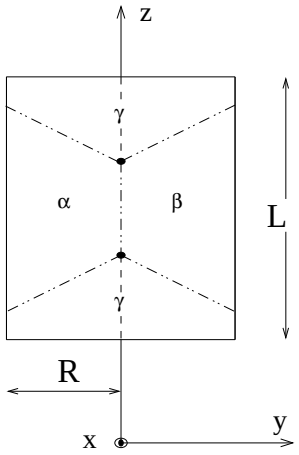

c)

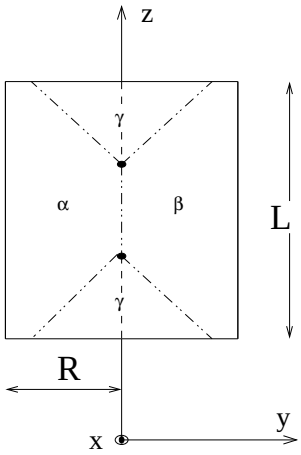

Figure 4:

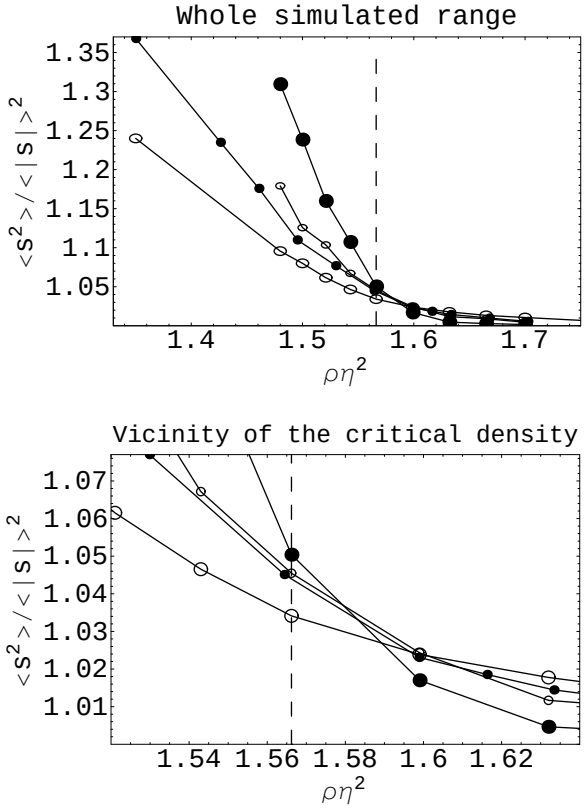
Whole simulated range
1.35
1.3
1.25
1.2
1.15
1.1
1.05
1.4
1.5
1.6
1.7
$\rho\eta^2$
$<s^2>/<|s|>^2$
Vicinity of the critical density
1.07
1.06
1.05
1.04
1.03
1.02
1.01
1.54
1.56
1.58
1.6
1.62
$\rho\eta^2$
$<s^2>/<|s|>^2$

Figure 5:

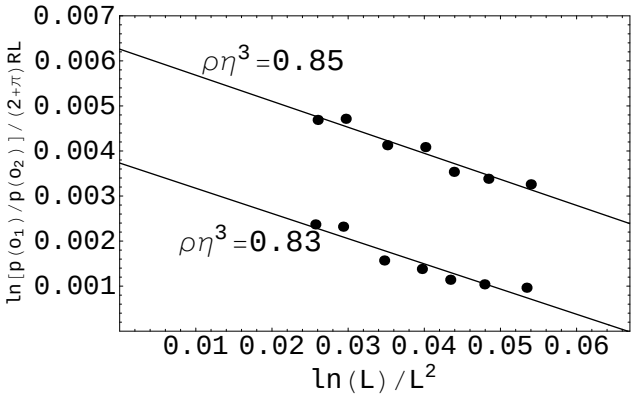
0.007
0.006
0.005
0.004
0.003
0.002
0.001
$\rho\eta^3$=0.85
$\rho\eta^3$=0.83
0.01 0.02 0.03 0.04 0.05 0.06
ln(L)/L^2
ln[p(o$_1$)/p(o$_2$)]/(2+π)RL

Figure 6:

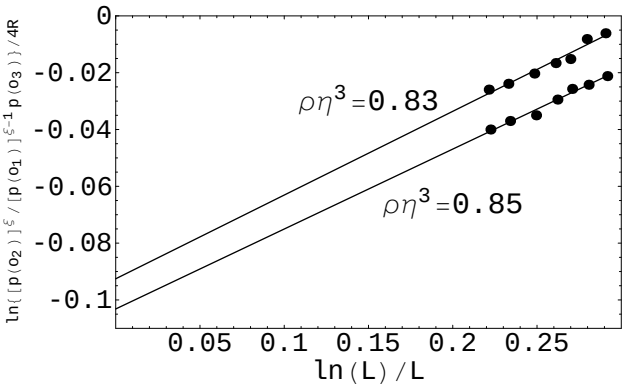
0
-0.02
-0.04
-0.06
-0.08
-0.1
0.05
0.1
0.15
0.2
0.25
ln(L)/L
ρη³=0.83
ρη³=0.85
ln{[p(σ2)]^ξ/[p(σ1)]^ξ-1 p(σ3)}/4R

Figure 7: